Change in Fine Structure of Nylon 6 Gut Yarn in Twisting, Annealing, and Untwisting Processes. I. Observation by WAXD, SAXD, and EM

ISHIO TSUJIMOTO, TERUO KUROKAWA, TOSHISADA TAKAHASHI, and KENSUKE SAKURAI, *Laboratory of Textile Physics, Fukui University, Fukui, Japan*

Synopsis

To obtain information on the change in fine structure of nylon 6 taking place during practical false-twisting processes, the manner of change in the three elemental processes, i.e., twisting, annealing, and untwisting, was studied. For simplicity, nylon 6 gut yarn was used instead of multifilament yarn. Wide- and small-angle x-ray diffraction (WAXD and SAXD) together with electron microscopy (EM) were used here. The degree of molecular orientation in the crystalline region of the twisted yarn gradually decreases with increase of the twist number (*TN*) in the region of $TN \gg 100$. The long spacing, determined by SAXD, of the twisted yarn increases with increase in *TN*. The increase in long spacing cannot be interpreted only by macroscopic strain or elongation of the yarn in the twisting process. This difference seems to arise from the contribution of the decrease of lateral size of lamellae to the average long spacing; therefore the increase in long spacing should be attributed to the elongation of the amorphous region, deduced from the crystallinity measured by WAXD and the long spacing diffraction. The angle between the streak line on the surface of twisted yarn observed by EM and the fiber axis agrees well with the twist angle of the yarn. The crystal lamellae are stacked normal to the streak line at the initial stage, i.e., at a low value of *TN*, but they begin to deviate from the normal direction with increase in *TN*, accompanied by their partial destruction. Based on SAXD and density measurements, the internal strain of yarn annealed after twisting is fully relaxed. When the yarn is untwisted after twisting and annealing, the crystal orientation recovers gradually to that of the untreated yarn. The chain axis within the lamellae in the center region of the yarn becomes nearly parallel to the fiber axis, but the chain axis in the outer region does not.

INTRODUCTION

Some studies on the macroscopic morphology that gives rise to the crimpness in a false-twisted yarn have been made.[1–3] Study of the fine structure in a false-twisted yarn in relation to the macroscopic structure will enable us to improve the property of a false-twisted yarn. However, it is difficult to obtain useful information from the small-angle x-ray patterns in cold-drawn nylon 6 multifilament yarns, because the SAXD pattern in these samples is obscured. In the present study, gut yarn of nylon 6 was used as the simplest case of a false-twisted yarn. Dividing the false-twisting process into three stages, i.e., (i) twisting process, (ii) heat set process, and (iii) untwisting process, the changes in fine structure in each stage were studied by means of wide- and small-angle x-ray diffraction together with electron microscopy.

Journal of Applied Polymer Science, Vol. 24, 2289–2301 (1979)

0021-8995/79/0024-2289$01.00

EXPERIMENTAL

Sample

A commercial nylon 6 gut yarn (Toray Co., 7000d, density 1.1472 g/cm^3) was used. For adequate lamellar structure, the sample was annealed and freely shrunk at 190°C for 10 min in a silicone oil bath; after annealing the silicone oil on the surface of the yarn was rinsed away by neutral detergent and dried in a desiccator. The three-stage procedure was carried out as follows.

A manual twisting apparatus was used to twist and to untwist the sample at room temperature. The sample was held by two cramps, one of which was manually rotated at a rate of 20 times per minute. Another cramp was devised so as to slide freely under the load of 265 g during twisting, and from the position of this cramp the change in sample length could be measured. The sample length in the twisting process was 30 cm. A heat-set procedure was carried out with constant length at 170°C for 15 min in an oven.

In the final stage of untwisting the postannealed sample was untwisted after it was kept at room temperature for 30 min.

X-Ray Measurements

Wide-angle x-ray diffractograms were obtained with a Rigaku Denki model D-IA x-ray diffractometer equipped with a scintillation counter. The x-ray source was nickel-filtered CuK_α radiation (40 kV, 20 mA). The diffraction intensity of the (200), (002), and (020) crystal planes along the azimuthal direction was measured to estimate the individual orientation angle of the a-, c-, and b-axes.[4] The degree of crystallinity based on the x-ray method was evaluated conveniently as follows. Namely, the sample was rotated stepwise by 5 degrees along the azimuthal direction from the equator up to the meridian. The scan was made in the scattering angle range 4–32° in each rotated condition. The measured intensity was separated into crystalline and amorphous components. The mean crystallinity was estimated by averaging these conveniently measured crystallinities. The crystallinity of heat-set samples was also calculated from the density measured at 20°C by flotation in a carbon tetrachloride–n-heptane mixture.[5]

The long spacing diffraction profiles were obtained with the small-angle x-ray goniometer. The x-ray source was nickel-filtered CuK_α radiation (Nippon Denshi, model JRX-12VA, 50 kV, 150 mA).

Electron-Microscopic Observations

Some samples were washed with tetrachloride to eliminate silicone oil if necessary, and a two-steps replica membrane was made in accordance with the usual method. The electron micrograph was obtained by use of a Nippon Denshi model JEM-200B.

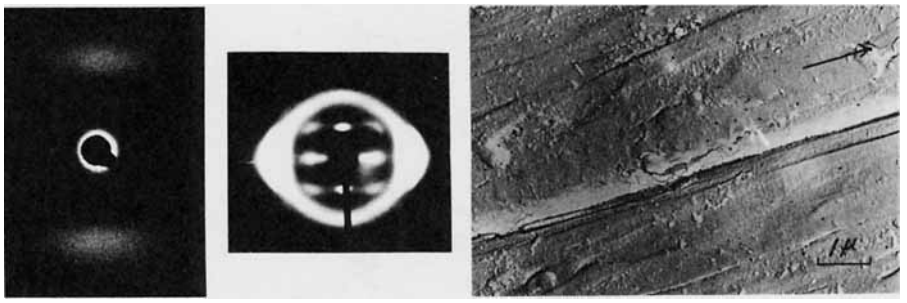

(a) (b) (c)

Fig. 1. SAXD, WAXD, and EM photographs of controlled sample: (a) SAXD; (b) WAXD; (c) EM (×14000). Arrow indicates the direction of fiber axis.

RESULTS AND DISCUSSION

Change of Fine Structure in the Twisting Process (First Stage)

Photographs of SAXD, WAXD, and EM of the controlled sample are shown in Figure 1. Both x-ray photographs show the fiber structure and discrete peaks on the meridian of the small-angle pattern which are layer-like. The EM gives the stacked lamellar structure though it is comparatively small, Figure 1(c). The changes of SAXD profiles with increase of twist are shown in Figure 2(a). The peak maximum of the profiles remains at almost the same scattering angle up to *TN* 150. With further increase of the twist to *TN* 200 and 250, the peak maximum shifts to a lower angle, i.e., the long spacing increases with increase in twist.

Now let us consider the change of long spacing, based on the modified two-phase model with the existence of microparacrystals (mPCs) at the end of the lamellae. They have an excess free lateral surface energy and are therefore more sensitive to temperature and stresses. The schematic drawing of Figure 3 shows four lamellae of thickness l_c and a length which is $1 - b$ of the two-phase model. Gaps of breadth b exist therefore between adjacent lamellae where vulnerable mPCs play an important role. Under stress or annealing the number of lamellae stacks remains constant (no selective melting of thinner lamellae occurs), but the mPCs at the end of the lamellae are destroyed and b increases. In this model the crystallinity X is given by

$$X = \frac{(1 - b)l_c}{l_c + l_a} \tag{1}$$

where l_c and l_a are the thickness of the crystalline and amorphous regions, respectively. With the first approximation the crystal thickness l_c would be roughly given by

$$l_c = X \cdot L_1 \tag{2}$$

where L_1 is the long spacing determined from the position of the peak maximum of SAXD profiles. The degree of crystallinity obtained from WAXD measurements and the change of crystal thickness calculated from eq. (2) are plotted against *TN* in Figures 4(a) and 4(b), respectively. The crystallinity tends to decrease slightly with increase in twist, but the crystal thickness can be regarded to be constant during twisting though there is a relatively large fluctuation.

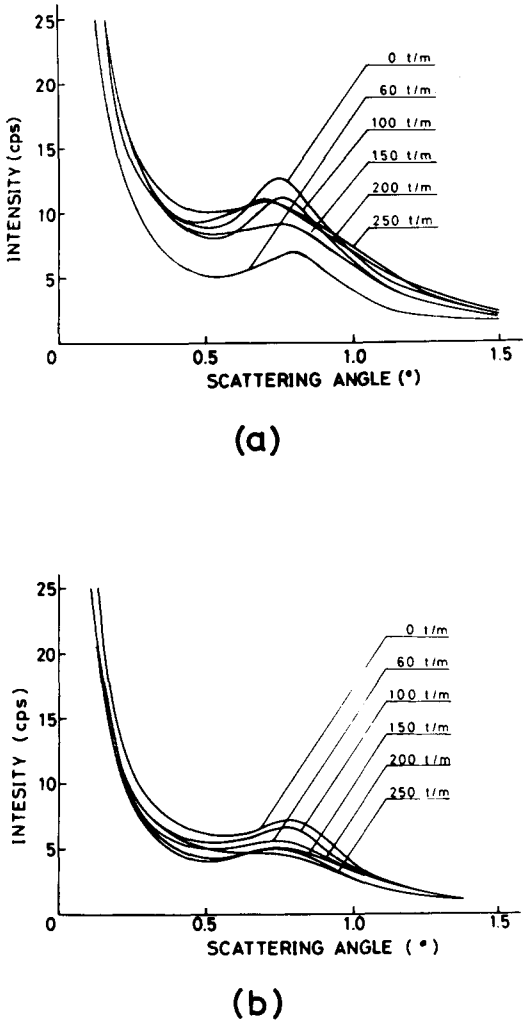

Fig. 2. Small-angle x-ray diffraction profiles: (a) as-twisted; (b) heat set after twist.

The SAXD mean long spacing L_1 in the given model is obtained by

$$L_1 = (1 - 2b)(l_c + l_a) + 2b \cdot 2(l_c + l_a)$$
$$= (1 + 2b)(l_c + l_a) \tag{3}$$

whereas the macroscopic length is proportional to

$$L_2 = l_c + l_a \tag{4}$$

Otherwise, the change in the long spacing L_2 (corresponding to the macroscopic length) in the twisting process is simply related to the macroscopic strain of the samples as follows;

$$L_2 = L_2^0(1 + e) \tag{5}$$

where L_2^0 and L_2 are the long spacings of the controlled and twisted samples, respectively, and e is the macroscopic strain of the twisted sample. The mac-

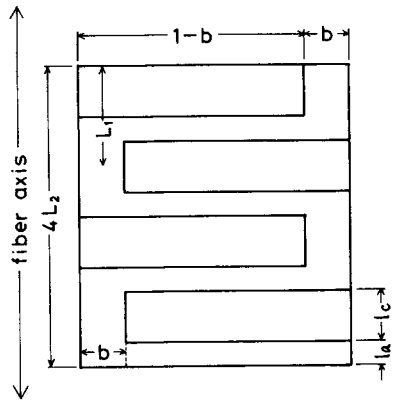

Fig. 3. Two-phase-model for the long spacing interference diffraction (including the existence of microparacrystals at the end of the lamellae).

roscopic strain e can be estimated by the change in sample lengths between those controlled and those untwisted after twisting. In Figure 5(a) the long spacings calculated from eq. (5) together with those observed are plotted against TN. The observed long spacing L_1 is a little larger than the calculated L_2 in the high-twisting region. A satisfactory explanation could be as follows. From eqs. (3) and (4) one obtains

$$\frac{dL_2}{L_2}\Big/\frac{dL_1}{L_1} = \frac{dL_2}{L_2}\frac{(1+2b)L_2}{(1+2b)dL_2 + 2L_2\,db}$$
$$= \left(1 + \frac{2db}{1+2b}\frac{L_2}{dL_2}\right)^{-1} \tag{6}$$

We obtain $dL_2/L_2 = 4\%$, $dL_1/L_1 = 12\%$ in Figure 5(a) and the crystallinity X shows large uncertainities for the sample before heat set, Figure 4(a). Thus, the following relation is obtained:

$$\frac{dL_2}{L_2}\Big/\frac{dL_1}{L_1} = \frac{1}{3} = \left(1 + \frac{2db}{(1+2b)0.04}\right)^{-1}$$

Hence, $db = 0.04(1 + 2b) > 4\%$. The crystallinity X then decreases after TN 250 some 2%, which agrees with the fact that a small decrease of some percent can be seen in Figure 4(a).

Under these considerations, in the twisting process the amorphous region slightly increases corresponding with the macroscopic strain of the samples and the lateral length of crystal lamellae decreases slightly, i.e., the mPCs at the end of the lamellae are somewhat destroyed by the applied shear force, while the change in crystal thickness may be negligible in this process.

SAXD photographs and the EM of the twisted samples are shown in Figures 6(a), 6(b), and 6(e). It should be noted that the small-angle x-ray pattern changes from layer-like to arc-like in the twisting process. This is more apparent in the twisted sample with TN 250 than in that with TN 150. It may suggest that the twisting does not affect the deformation of lamellar structure in the center region of the sample and that the larger deformation takes place in the outer layer. In the SAXD pattern, this deformation brings out a so-called two-point pattern from the center region and a four-point one from the outer region of the yarn.

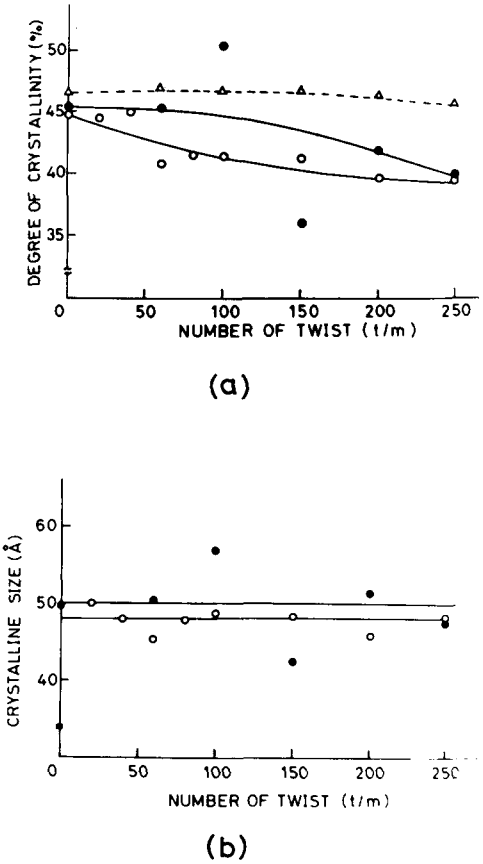

Fig. 4. Crystallinity and crystal size before and after heat set as function of twist number. (○) before heat set; (●) after heat set; (△) after heat set (density).

It could be considered that the arc-like pattern is the result of an overlap of the two regions. These phenomena can be also recognized from the EM of the twisted sample with *TN* 150, Figure 6(e). In the low-twist region the crystal lamellae incline as one body with the direction perpendicular to the streak, but in the high-twist region they incline gradually from the direction perpendicular to the streak accompanied by the partial destruction of lamellae due to the shear force during twisting.

In order to follow the change in crystal orientation during the twisting process, the azimuthal diffraction intensity of the (200), (002), and (020) planes was measured. It is seen from Figure 7 that the peak intensity decreases and the width of the profile broadens with increase in twist. This fact indicates the decrease in the degree of crystal orientation with increase in twist. In addition, it is noted that the intensity curve of the (002) plane changes shape, i.e., from a single-peak to a double-peak profile with increase in twist. This phenomenon will be discussed in more detail in the next study which used the microbeam x-ray technique to examine changes in fine structure in the local positions within a sample.

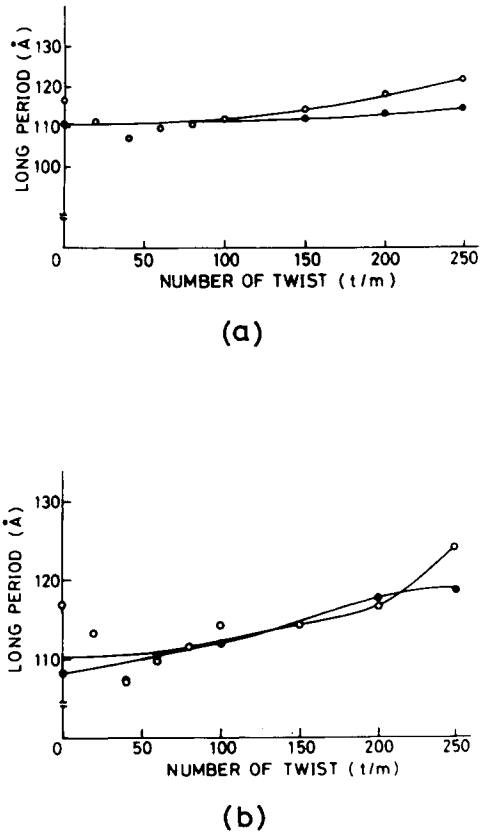

Fig. 5. Long spacing as function of twist number: (a) observed value (○) and calculated value (●) from the macroscopic strain; (b) before heat set (○) and after heat set (●).

The quantitative estimation of crystal orientation is usually performed by use of the orientation function as proposed by Hermans[4] and/or Stein.[6] The orientation function f is defined by

$$f = \frac{1}{2}(3\langle\cos^2\phi\rangle - 1) \tag{7}$$

$$\langle\cos^2\phi\rangle = \frac{\int_0^{\pi/2} I(\phi)\cos^2\phi\sin\phi\,d\phi}{\int_0^{\pi/2} I(\phi)\sin\phi\,d\phi} \tag{8}$$

where ϕ is the angle between the crystal axis and the fiber axis and $I(\phi)$ is the intensity distribution function along the azimuthal direction. Here, we define the mean orientation angle as the value of ϕ calculated from $\langle\cos^2\phi\rangle$ given by eq. (8). Clearly, this value has no significant physical meaning except for the special case of complete orientation, but it would be a measure of the change in crystal orientation such as f and $\langle\cos^2\phi\rangle$. Namely, as the mean orientation angle decreases from 90° in the case of the a- and c-axes and as it increases from 0° in the case of the b-axis, the crystal orientation deteriorates.

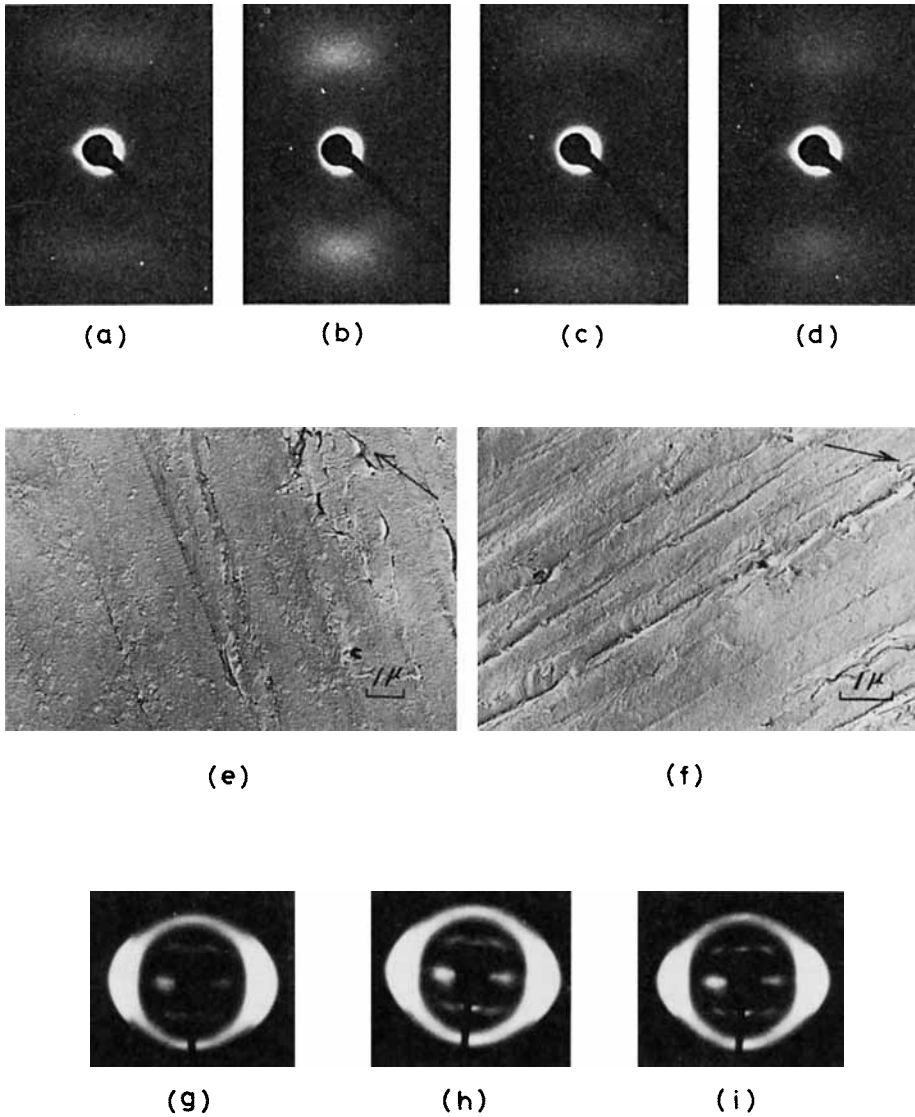

Fig. 6. SAXD, WAXD, and EM photographs under various conditions: (a) and (b) SAXD, as-twisted with *TN* 150 and 250; (c) SAXD, heat set for sample (b); (d) SAXD, untwisted by 100% for sample (c); (e) and (f) EM corresponding to (a) and (d); (g), (h), and (i) WAXD, untwisted by 80, 100, and 120% for sample (c), respectively.

The mean orientation angles of the a-, c-, and b-axes calculated from the intensity curves shown in Figure 7 are plotted against *TN* in Figure 8(a). The orientation angle of the a-axis scarcely changes up to *TN* 80 and gradually decreases in the region above it. The degree of c-axis orientation begins to decrease at *TN* 60, lower than in the case of the a-axis, and the rate of change is faster than that of the a-axis. This behavior could be explained by the well-known fact that nylon 6 (α-form) has a hydrogen bond in the a-axis direction and that there is only a weak bond due to van der Waals forces in the c-axis direction. On the other hand, the degree of orientation of the b-axis starts to decrease in the region

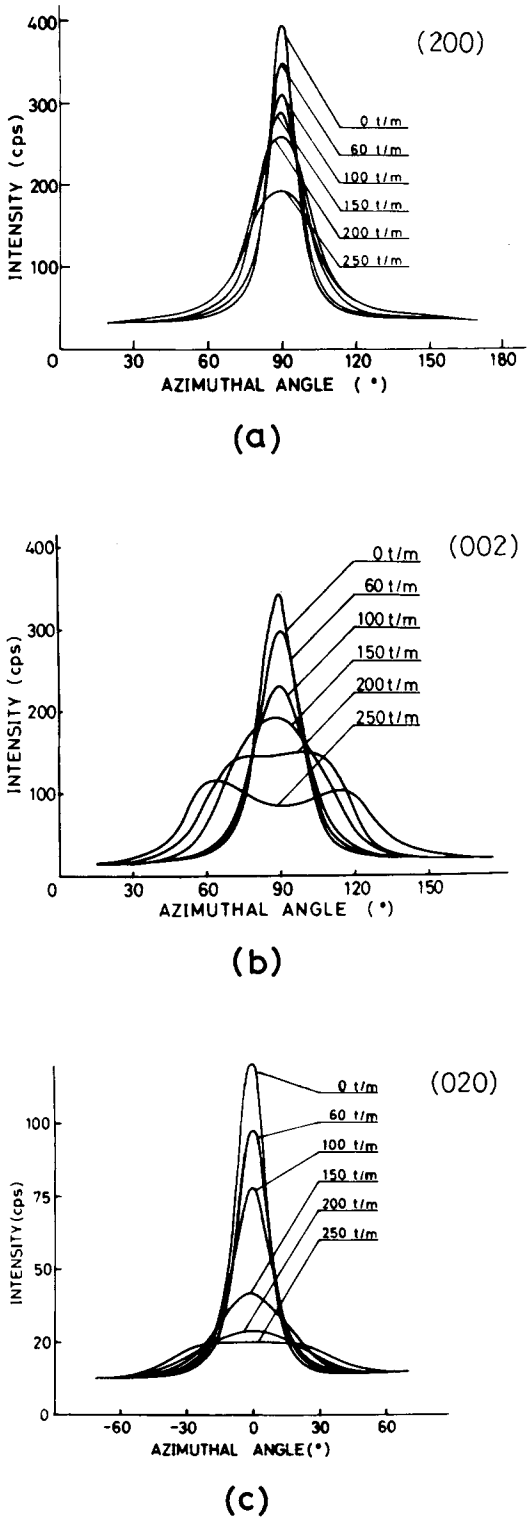

Fig. 7. Azimuthal intensity profiles of (200), (002), and (020) crystal planes.

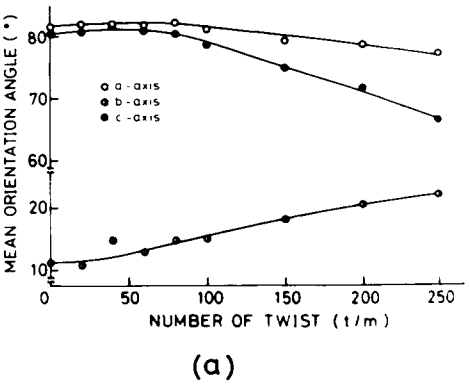

(a)

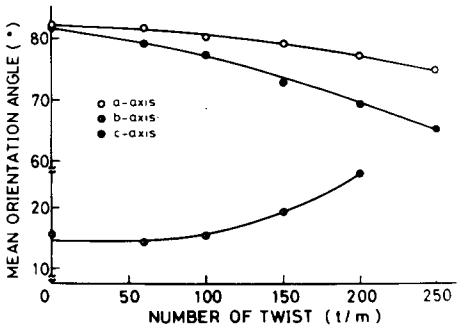

(b)

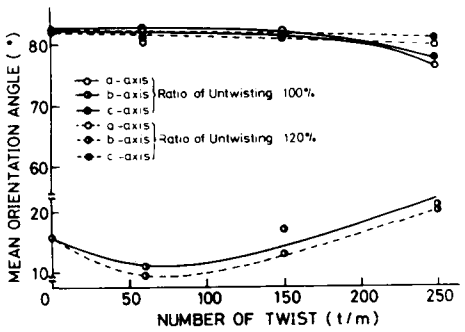

(c)

Fig. 8. Mean orientation angle estimated from Fig. 7 as function of twist number: (a) as-twisted; (b) heat set; (c) untwisted.

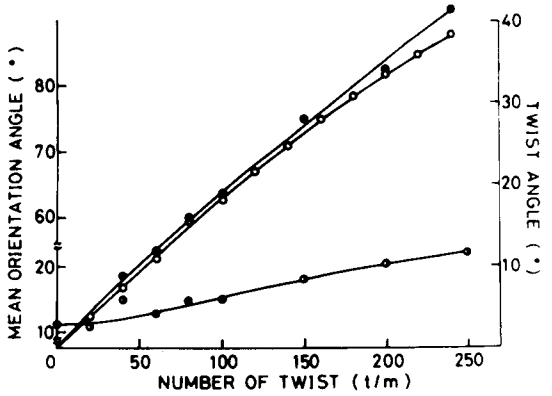

Fig. 9. Changes of twist angle, (○); inclination angle of streak line (EM), (●); and the mean orientation angle of b-axis, (◐), during twisting.

of relatively lower twist. In Figure 9 the change of twist angle on the surface of the yarn measured by the optical microscope and the change in the inclination angle of the streak obtained from the EM are shown together with that of the mean orientation angle of the b-axis. The changes in the surface twist angle and the inclination angle of streak show good agreement, while the orientation angle of the b-axis scarcely changes in the lower-twist stage. These facts confirm the explanation of the mechanism of lamellar deformation mentioned above.

Effect of Heat Set After Twisting (Second Stage)

The SAXD profiles of the heat-set samples are shown in Figure 2(b). Comparing the peak intensities of samples before and after heat set, shown in Figures 2(a) and 2(b), a decrease in intensity was found after annealing. According to the paracrystalline model proposed by Hosemann et al.,[7] the diffraction intensity I is given by

$$I = K(\Delta\rho)^2 \langle f(s) \rangle^2 Z(s) \tag{9}$$

where s is the reciprocal vector, $\Delta\rho$ is the density difference between the crystalline and amorphous regions, $\langle f(s) \rangle^2$ is the shape factor, $Z(s)$ is the lattice factor, and K is a constant. The reduction of intensity will be discussed on the basis of this equation. There is little change of long spacings in both samples before and after annealing shown in Figure 5(b), in which the long spacing is plotted as a function of TN. There are no large differences between the crystallinities of the samples shown in Figure 4(a), together with that calculated from the density shown by the dotted line. As the shape factor $\langle f(s) \rangle^2$ is directly related to the crystallinity and the long spacing but neither of them changes largely between samples before and after annealing, the effect of $\langle f(s) \rangle^2$ on the intensity may be negligible. As seen in Figures 2(b) and 2(a), the width of the profile becomes broader compared with the sample before annealing. The profile width is related to the lattice factor $Z(s)$, and the width broadening must bring about a reduction in intensity. In the preceding process of twisting, the nonuniform deformation of crystal lamellae occurs in the high-twist region, and when this sample was annealed at constant length, the distribution of crystal lamellae as a scattering unit may broaden (being ununified still further), accompanied by

relaxation or more stable rearrangement of the amorphous chains. Another possibility for the reduction in intensity is that in the sample annealed at constant length the more stable rearrangement of amorphous chains might cause better packing or increase in amorphous density, and thus the density difference between crystalline and amorphous regions decreased resulting in a reduction of intensity. With regard to the shape of the SAXD pattern, it is seen from Figures 6(c) and 6(b) that the curvature of the arc-like pattern slightly recovers with the reduction in intensity as compared with the sample before annealing.

The mean orientation angles of the crystal axes of the heat-set sample are plotted as a function of *TN* in Figure 8(b), from which it is found that the mean orientation angle of the *a*- and *c*-axes starts to decrease at the lower-twist region compared with those in the sample before annealing. This indicates a worse orientation of the *a*- and *c*-axes after annealing. On the other hand, the orientation angle of the *b*-axis remains at almost the same value up to *TN* 100. This means that the inclination of the *b*-axis recovers after annealing. However, in the higher-twist region than *TN* 150, the effect of annealing is not appreciable. As to the effect of heat set, the crystal orientation becomes worse accompanied by the relaxation of internal strain to result in a more stable structure.

Change of Fine Structure in the Untwisting Process (Third Stage)

The SAXD pattern and the EM are shown in Figures 6(d) and 6(f), respectively, in the untwisted sample with a history of *TN* 250 and heat set. Figure 6(d) shows the layer-like pattern on the meridian which may suggest the recovery of inclination of the *b*-axis toward the fiber axis. The EM shows that the crystal lamellae are bent and the streak does not recover parallel to the fiber axis to be kept oblique, while the crystal lamellae are not bent before untwisting. On untwisting the sample over 100%, such a bend in the crystal lamellae proceeds toward the interior region of the sample. This could account for the fact that crimpness is characteristically brought about by a false twist procedure. Figures 6(g), 6(h), and 6(i) show the WAXD photographs when the sample was untwisted to some extent, i.e., by 80, 100, and 120%, respectively. From these figures the orientation of the (200) and (002) planes is improved with increase in untwist. The mean orientation angles of the crystal axes in the samples untwisted by both 100% and 120% are plotted as a function of *TN* in Figure 8(c). The more the sample was untwisted, the more the orientation of the crystal axes recovered. The orientation of the *a*- and *c*-axes almost completely recovered when the sample was untwisted in the region up to *TN* 150. On the other hand, the orientation of the *b*-axis approaches the direction of the fiber axis at *TN* 60, but the degree of recovery decreases as *TN* increases further.

CONCLUSIONS

When the sample is twisted, the crystal orientation does not change up to *TN* 100; and thereafter it tends to decrease. The long spacing tends to increase with increase in the twist, the value of which is little larger than that calculated from the macroscopic strain of the sample. The increase in long spacing is not attributable to the crystalline region but mainly to the extension of the amorphous region corresponding to the macroscopic strain and the effect of the destruction

of mPCs at the end of lamellae on the mean long spacing. The angle of streak line on the surface is in a good agreement with that of the twist. With regard to the effect of the twisting on the fine structure, the outer regions in the sample are influenced most. The crystal lamellae are perpendicular to the streak in the region of low twist but gradually incline, accompanied by partial destruction of the lamellae as the number of twists increases.

When the sample is annealed after twisting, the structure would be stabilized accompanied by the relaxation of interior strain that takes place during twisting.

When the heat-set sample is untwisted, the crystal orientation is likely to recover and the degree of recovery is advanced with increase in untwist. The crystal lamellae are kept bent themselves in the outer region of the sample untwisted by 100%. As the sample is further untwisted over 100%, the bend of the crystal lamellae prevails in the interior of the sample. Finally, it may be considered that the bend of the crystal lamellae might be the cause of the crimpness in a false-twisted yarn.

The authors wish to express thanks to the Department of Textile and Industrial Research for permission to use the SAXD apparatus to perform the present work and are also grateful for the technical assistance provided by Mr. M. Tsuji.

References

1. S. Kakiage, *J. Text. Machin. Soc., Jpn.* **16,** T123 (1963).
2. K. Fuchino, *Sen-i Gakkaishi, Jpn.* **12,** T887 (1956).
3. H. Nakazato, *Sen-i Gakkaishi, Jpn.* **14,** T15 (1958).
4. P. H. Hermans, *Contribution to the Physics of Cellulose Fibers,* Elsevier, Amsterdam, 1946.
5. L. E. Alexander, *X-Ray Diffraction Methods in Polymer Science,* Wiley, New York, 1969.
6. R. S. Stein, *J. Polym. Sci.,* **31,** 327 (1958).
7. R. Hosemann and S. N. Bagchi, *Direct Analysis of Diffraction by Matter,* North-Holland, Amsterdam, 1962.

Received June 1, 1979
Revised July 24, 1979